Journal of Solid Mechanics Vol. 12, No. 3 (2020) pp. 586-599
DOI: 10.22034/jsm.2019.1875642.1476

An Analytical Solution on Size Dependent Longitudinal Dynamic Response of SWCNT Under Axial Moving Harmonic Load

F. Khosravi [1], M. Simyari [2], S.A. Hosseini [3,*], M. Ghadiri [4]

[1]*Department of Aerospace Engineering, K.N. Toosi University of Technology, Tehran, Iran*
[2]*Department of Mechanical Engineering, University of Tehran, Tehran, Iran*
[3]*Department of Industrial, Mechanical and Aerospace Engineering, Buein Zahra Technical University, Buein Zahra, Qazvin, Iran*
[4]*Faculty of Engineering, Department of Mechanics, Imam Khomeini International University, Qazvin, Iran*

Received 11 June 2020; accepted 12 August 2020

ABSTRACT

The main purposes of the present work are devoted to the investigation of the free axial vibration, as well as the time-dependent and forced axial vibration of a SWCNT subjected to a moving load. The governing equation is derived through using Hamilton's principle. Eringen's nonlocal elasticity theory has been utilized to analyze the nonlocal behaviors of SWCNT. A Galerkin method based on a closed-form solution is applied to solve the governing equation. The boundary conditions are considered as clamped-clamped (C-C) and clamped-free (C-F). Firstly, the nondimensional natural frequencies are calculated, as well as the influence of the nonlocal parameter on them are explained. The results of both boundary conditions are compared together, and both of them are compared to the results of another study to verify the accuracy and efficiency of the present results. The novelty of this work is related to the study of the dynamic forced axial vibration due to the axial moving harmonic force in the time domain. The previously forced vibration studies were devoted to the transverse vibrations. The effect of the geometrical parameters, velocity of the moving load, excitation frequency, as well as the small-scale effect, are explained and discussed in this context. According to the lack of accomplished studies in this field, the present work has the potential to be used as a benchmark for future works.

Keywords : Moving load; Size dependent; Axial vibration; Free vibration; Forced vibration; Galerkin method; Harmonic load.

1 INTRODUCTION

THE discovery of fullerenes [1, 2] and CNTs [3-5] since 1991, made the researchers focus on the two different allotropes of carbon, including almond and graphene [6]. Carbon nanotubes (CNTs) have considerable mechanical, thermal [7], and electrical [7, 8] properties , as well as high strength, low density [4, 9]. Carbon

*Corresponding author.
E-mail address: hosseini@bzte.ac.ir (S.A. Hosseini).

nanotubes are layers of rolled-up graphene[10], which depending on their applications, are divided into three different types. CNTs are composed of one layer graphene or more, which are known as single-walled (SWCNT) and multi-walled (MWCNT) carbon nanotubes, respectively [11]. SWCNTs and MWCNTs have three different structures, including zigzag, chiral, and armchair structures [12]. The production of carbon nanotubes is limited to three methods, including electric-arc discharge, laser ablation, and CVD [13]. CNTs are utilized in different branches such as the vibration of FG-CNT [14, 15], sandwich plates [16, 17], etc. The applications of CNT can be summarized in Nano biology [18, 19], Nano devices [20, 21], and nanocomposites [22, 23]. The local continuum theory cannot be qualified for the nanoscale structures [24-29]. To do that, Eringen's nonlocal elasticity theory [30, 31], has been selected. However, there are different other theories for small-scale studies [32-41]. Xu et al. [42] investigated the effect of the nonlinear van der Waals forces between layers in coaxial and non-coaxial free vibration of the DWCNT. Lee and Chang [43] analyzed the vibrational behavior of the SWCNT conveying viscous-fluid surrounded by an elastic medium. Moradi-Dastjerdi et al. [44] worked on the free vibration analysis of FG-nanocomposite reinforced by a CNT using an axisymmetric model. Pourseifi et al. [45] utilized an active control vibration of a simply supported CNT under a moving nanoparticle. Mahdavi et al. [46] studied the effect of the nonlinear interaction van der Waals forces between adjacent tubes and elastic polymer matrix in free non-coaxial responses of MWCNT. In addition, the axial force is applied to evaluate the variation of the responses. Kiani [47] modeled a tapered nanowire, which variates in radii and cross-sectional area linearly, and assessed the accuracy by Fredholm theorem. Timoshenko beam theory is utilized by Askari et al. [48] to analyze the nonlinear vibration of nanowires with the various cross-sectional area along with Galerkin and energy methods as analytical methods. Ansari et al. [49] modeled FG-CNTRC annular sector plates under the thermal loading embedded in an elastic medium to analyze the buckling and natural frequencies. Yas and Heshmati [50] investigated the FG nanocomposite beams, which was reinforced by randomly oriented CNT subjected by transverse moving force. The forced vibration of a SWCNT under a moving harmonic load based on Euler-Bernoulli theory was studied by Şimşek [51]. Malekzadeh and Zarei [52] carried out the free vibration of quadrilateral plates laminated by composite layers with CNT reinforced using first-order shear deformation theory. Joshi et al. [53] simulated SWCNT under an attached mass for bridged and fixed-free end conditions using a FEM approach to calculate the resonant frequencies by variation the value of the mass and length. Aydogdu [54] used Eringen nonlocal elasticity theory to obtain the axial natural frequencies of a CNT surrounded by an elastic medium using Nano rod model. In another study, Aydogdu [55] investigated the effect of the van der Waals force on the axial vibration of DWCNT, and showed the influence of the van der Waals force on the axial vibration of CNT. The small-scale effect, the influence of the stiffness parameter, and geometrical parameters are illustrated. Murmu and Adhikari [56] studied the axial vibration of a double-Nano rod-system coupled with longitudinally directed springs using Eringen theory to show the effect of the nonlocality on the axial vibration of DNRS. Free axial vibration of a tapered AFG Nano rod for two various end supports, including C-C and C-F boundary conditions, are investigated by Şimşek [57]. The cross-sectional area was changed linearly and sinusoidal, and results compared with those obtained from other studies. Murmu and Adhikari [58] worked on the instability of the double-nanobeams, which was elastically connected to evaluate the small-scale effect. Also, the stiffness of the medium on the instability of the in-phase and out-phase buckling, are studied when one of the Nano beams are fixed. Danesh et al. [59] investigated the axial vibration of a tapered nanorod based on nonlocal elasticity theory and differential quadrature method as an analytical method. In addition, it was proved that the nonlocal parameter makes the non-dimensional frequency decreases. Filiz and Aydogdu [60] considered CNT heterojunctions, and used a Nano rod model to analyze the free axial vibration for different values of CNT's length, along with the first segment's length, and inferred suitable parameters cause good vibrational properties. The axial responses of the hetero-junction CNTs were accomplished by Mohammadian et al. [61]. Their model also considered other nanostructures. The effect of the small-scale parameter, the elastic ratio, connecting region, and mass sensors on the frequency demonstrated. Liu et al. [62] analyzed the distributed axial and torsional vibration simultaneously. Aydogdu and Filiz [63] modeled CNT-based mass sensors using nonlocal elasticity theory to show the effect of the nonlocal parameter, attached mass, and length. Bouadi et al. [64] utilized a new nonlocal higher-order shear deformation theory with new displacement component to study the buckling properties of a single graphene sheet. Cherif et al. [65] modeled an Euler-Bernoulli Nano beam to investigate the vibrational behavior of the SWCNT embedded in an elastic medium, based on the differential transform method. Kadari et al. [66] carried out the buckling behavior of the orthotropic nanoplates embedded in elastic foundations based on a new hyperbolic plate theory and nonlocal small scale effects. Yazid et al. [67] established a new refined plate theory considering the small-scale effect to analyze the buckling of an orthotropic Nanoplate embedded in an elastic foundation. Youcef et al. [68] employed a non-classical model considering the surface stress effects to study the free vibrational behavior of the Nano beams. Draoui et al. [69] used the first-order shear deformation plate theory to study the dynamic and static behavior of the carbon nanotube-reinforced composite sandwich plates with two various sandwich plates and

distribution uniaxially aligned reinforced materials. Mokhtar et al. [70] accomplished the buckling behavior of a single layer graphene sheet considering the shear deformation effect based on nonlocal elasticity theory. Boutaleb et al. [71] analyzed the natural responses of the rectangular nanoplates based on a simple nonlocal quasi 3D higher shear deformation theory. Karami et al. [72] employed a novel size-dependent quasi-3D plate theory to work on a wave dispersion of FG Nanoplate embedded in an elastic foundation under a hydrothermal environment. Karami et al. [73] established the three-dimensional elasticity theory concerning strain gradient theory with two scale coefficients to study the mechanical characteristics of FG spherical nanostructures, and their results were compared with experimental works. Also, a variational behavior was investigated by Karami et al. [74] to study the wave dispersion of doubly-curved Nano shells using a new size-dependent higher-order shear deformation theory based on strain gradient theory. They demonstrated the influences of nonlocal strain gradient theory, wave number, and material properties on wave frequency. Bellifa et al. [75] analyzed the nonlinear post buckling behavior of clamped-clamped and simply supported Nano beams based on the zeroth-order shear deformation theory and Eringen's nonlocal elasticity approach, considering the shear deformation effect. Karami et al. [76] evaluated the wave propagation of anisotropic nanoplates due to the triaxial magnetic field based on the nonlocal strain gradient as well as the three-dimensional elasticity theory. Bouafia et al. [77] employed a nonlocal quasi-3D theory considering the shear deformation and thickness stretching effects to analyze the bending and free flexural vibration of FG Nano beams based on Eringen's nonlocal elasticity theory. Zemri et al. [78] utilized a shear deformation beam theory to analyze the bending, buckling, and vibration of FG Nano beam under the stress-free boundary conditions based on nonlocal shear deformation beam model and Eringen's nonlocal elasticity theory.

Based on the author's knowledge, the dynamic axial vibration under the axial moving load has not been done yet. Therefore, the time-dependent forced vibration of the SWCNT under an axial moving harmonic force subjected to any point of the body is investigated in this paper. Hamilton's principle is used to derive the equation and corresponding boundary conditions. The small-scale effect has been shown by Eringen's nonlocal elasticity theory. An analytical method, called Galerkin method is applied to solve the reduced-order equation. The clamped-clamped and clamped-free boundary conditions are utilized. In free vibration, the nondimensional axial natural frequencies for variant nonlocal parameters is studied. In time-dependent axial vibration, the effect of the moving load velocity, geometrical parameters, excitation frequency, and nonlocal parameter are investigated. The results can be used as good comparative cases for future studies in this filed.

2 NONLOCAL SWCNT MODEL

SWCNT under an axial moving force at any point of the body has been depicted in Figs. 1 and 2. The parameters l ,v_0 ,F_t and δ represent the length, velocity of the moving load, time-dependent force and Dirac delta, respectively. The axial axis is considered in the direction of the x-axis.

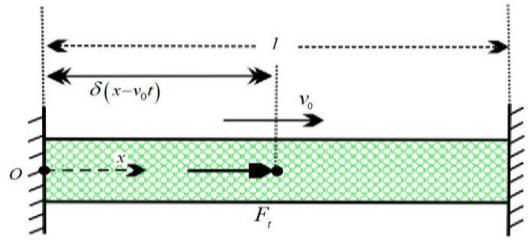

Fig.1
SWCNT under a moving force for clamped-clamped boundary condition.

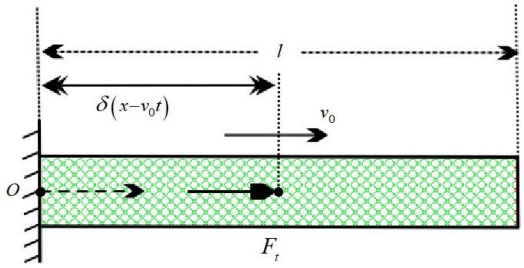

Fig.2
SWCNT under a moving force for clamped-free boundary condition.

Fig. 1 shows SWCNT for clamped-clamped boundary condition, while Fig. 2 indicates SWCNT for clamped-free boundary condition. The displacement field due to the axial deflection can be written as:

$$\begin{aligned} u_x &= u\left(x,t\right) \\ u_y &= 0 \\ u_z &= 0 \end{aligned} \tag{1}$$

where $u\left(x,t\right)$ is the only expression of the displacement at point x along the x-axis. The components of the strain tensor are given by:

$$\begin{aligned} \varepsilon_{xx} &= \frac{\partial u}{\partial x} \\ \varepsilon_{yy} &= \varepsilon_{zz} = \varepsilon_{xz} = \varepsilon_{xy} = \varepsilon_{xz} = \varepsilon_{yz} = 0 \end{aligned} \tag{2}$$

The governing Equation for a SWCNT subjected to the axial force can be defined as:

$$\frac{\partial N}{\partial x} = \rho A \frac{\partial^2 u}{\partial t^2} - f_t\left(x,t\right) \tag{3}$$

In which N represents the nonlocal axial force per unit length. Parameter A denotes the cross-sectional area and is equal to:

$$A = \pi\left(R_{out}^2 - R_{in}^2\right) \tag{4}$$

where R_{out} and R_{in} represent the outer and inner radii of CNT, respectively. The corresponding boundary condition is equivalent to:

$$\left(N -\right)\delta u\Big|_0^l = 0 \tag{5}$$

The nonlocal constitutive stress-strain equation based on Eringen's nonlocal elasticity theory can be formulated as:

$$\sigma_{kl} - \left(e_0 a\right)^2 \frac{\partial^2 \sigma_{kl}}{\partial x^2} = E\,\varepsilon_{kl} \tag{6}$$

From above, σ_{kl} represents the nonlocal stress, and ε_{kl} denotes the nonlocal strain tensor. For the axial vibration of uniform SWCNT Eq. (6) changes into the following statement:

$$\sigma_{xx} - \left(e_0 a\right)^2 \frac{\partial^2 \sigma_{xx}}{\partial x^2} = E\,\varepsilon_{xx} \tag{7}$$

where E is Young's modulus of elasticity. By integrating Eq. (7) based on the cross-sectional area, the following statement can be taken:

$$N - \mu \frac{\partial^2 N}{\partial x^2} = N_x^l \tag{8}$$

where N_x^l is the local axial force per unit length, and is equivalent to:

$$N_x^l = \int_A \sigma_{xx} dA = EA\,\varepsilon_{xx} \tag{9}$$

Replacing the first derivative of Eq. (3) into Eq. (8) leads to:

$$N - (e_0 a)^2 \left(\rho A \frac{\partial^3 u}{\partial x\, \partial t^2} - \frac{\partial f_t(x,t)}{\partial x} \right) = EA \frac{\partial u}{\partial x} \tag{10}$$

As a final step, to obtain the equation of motion for SWCNT under the axial displacement, the first derivative of Eq. (10) should be substituted into Eq. (3) as below:

$$(e_0 a)^2 \left(\rho A \frac{\partial^4 u}{\partial x^2 \partial t^2} - \frac{\partial^2 f_t(x,t)}{\partial x^2} \right) - \rho A \frac{\partial^2 u}{\partial t^2} + EA \frac{\partial^2 u}{\partial x^2} + f_t(x,t) = 0 \tag{11}$$

If $e_0 a$ set to be zero, Eq. (11) will turn into the following local form:

$$EA \frac{\partial^2 u}{\partial x^2} - \rho A \frac{\partial^2 u}{\partial t^2} + f_t(x,t) = 0 \tag{12}$$

3 ANALYTICAL METHOD

3.1 Free axial vibration

In free axial vibration, the force should be omitted (i.e., $f_t(x,t)$). So the equation of motion can be rewritten as:

$$(e_0 a)^2 \left(\rho A \frac{\partial^4 u}{\partial x^2 \partial t^2} \right) - \rho A \frac{\partial^2 u}{\partial t^2} + EA \frac{\partial^2 u}{\partial x^2} = 0 \tag{13}$$

The Galerkin method is utilized for discretizing and division of the equation of motion into two different parts as follows:

$$u(x,t) = \sum_{n=1}^{\infty} U_n(x) \sin \omega t \tag{14}$$

where $U_n(x)$ represents the *nth* mode shape corresponding to the axial vibration, and the time-dependent part is considered sinusoidal.

$$EA\,U_n'' - (e_0 a)^2\, \omega^2 U_n'' (\rho A) + \rho A\, \omega^2 U_n = 0 \tag{15}$$

The mode shape for two states of the boundary conditions has the following format.

$$U_n(x) = B_n \sin(Px) \tag{16}$$

The natural frequency of axial vibration can be obtained as:

$$\omega_n = \sqrt{\frac{C_2}{\left(1/P^2 + (e_0 a)^2\right)}} \tag{17}$$

In which the coefficient in Eq. (17) is equivalent to $C=\sqrt{E/\rho}$. In addition, the coefficient for the C-C and C-F boundary conditions, respectively, can be stated as:

$$P=n\pi/l \tag{18}$$

$$P=(2n-1)\pi/2l \tag{19}$$

By applying Eqs. (18) and (19) into Eq. (17), the following expressions result in:

$$\bar{\omega}_n=\sqrt{\frac{(n\pi)^2}{\left(1+(e_0a)^2(n\pi/l)^2\right)}} \tag{20}$$

$$\bar{\omega}_n=\sqrt{\frac{((2n-1)\pi/2)^2}{\left(1+(e_0a)^2((2n-1)\pi/2l)^2\right)}} \tag{21}$$

where Eq. (20) represent the nondimensional natural frequency for C-C boundary condition, while Eq. (21) is used for C-F boundary condition.

3.2 Galerkin method for dynamic axial vibration

A Galerkin method is used as an analytical method to convert the higher-order of governing equation to ODE one. The unknown axial deflection can be stated as:

$$u(x,t)=\sum_{n=1}^{\infty}U_n(x)q_n(t) \tag{22}$$

In which $q_n(t)$ denotes the unknown time-dependent generalized coordinates. Substitution of Eqs. (22) and (16) into Eq. (11) results in:

$$EAP^2\sum_{n=1}^{\infty}U_n(x)q_n(t)+\left(e_0a^2\right)\left(\sum_{n=1}^{\infty}(\rho A)P^2U_n(x)\ddot{q}_n(t)+\frac{\partial^2 f_t(x,t)}{\partial x^2}\right)+\sum_{n=1}^{\infty}(\rho A)U_n(x)\ddot{q}_n(t)-f_t(x,t)=0 \tag{23}$$

Multiplication of Eq. (23) with $q_n(t)$ and subsequently integrating it over the length's span ($0<x<l$) yields:

$$\begin{aligned}&EAP^2q_n(t)\int_0^l U_n(x)U_m(x)dx+\int_0^l\left((e_0a)^2\frac{\partial^2 f_t(x,t)}{\partial x^2}-f_t(x,t)\right)U_m(x)dx\\&+\rho A\ddot{q}_n(t)\int_0^l U_n(x)U_m(x)dx+(\rho A)P^2\left(e_0a^2\right)\ddot{q}_n(t)\int_0^l U_n(x)U_m(x)dx=0\end{aligned} \tag{24}$$

The normalized mode shape of CNT to satisfy the orthogonality relationships can be expressed as:

$$\int_0^l U_n^2(x)dx=1 \tag{25}$$

From Eq. (25), the coefficient B_n can be obtained by multiplication of mode shapes together as follows:

$$B_n^2\int_0^l\sin^2(Px)dx=1 \tag{26}$$

Solving Eq. (26) in the length domain, leads to:

$$B_n = \sqrt{2/l} \qquad n = 1,2,... \tag{27}$$

It leads to rewritten the mode shape from Eq. (16) as:

$$U_n(x) = \sqrt{2/l}\sin(Px) \tag{28}$$

According to the normalized mode shape in Eq. (25), Eq. (24) can be rewritten as:

$$\rho A\left(1+(e_0a)^2(P)^2\right)\ddot{q}_n(t)+EA(P)^2 q_n(t)=\int_0^l\left[f_t(x,t)-(e_0a)^2 f_t''(x,t)\right]U_m(x)dx \tag{29}$$

The simplified form of Eq. (29) can be stated as:

$$\ddot{q}_n(t)+\lambda_n^2 q_n(t)=Y_n F_n(t) \tag{30}$$

where the nonlocal natural frequency and coefficient can be expressed as:

$$\lambda_n = \frac{\omega_n}{P^2E/P\left(1+e_0a\right)^2P^2} \tag{31}$$

$$Y_n = \frac{1}{\rho A\left(1+(e_0a)^2P^2\right)} \tag{32}$$

$F_n(t)$, which is called the generalized force in *nth* mode, can be determined as:

$$F_n(t)=Y_n\int_0^l\left(f_t(x,t)-(e_0a)^2\frac{\partial^2 f_t(x,t)}{\partial x^2}\right)U_m(x)dx \tag{33}$$

The unknown time-dependent generalized coordinates disregarding the initial condition can be obtained as:

$$q_n(t)=\frac{Y_{1n}}{\lambda_n}\int_0^t F_n(\tau)\sin\lambda_n(t-\tau)d\tau \tag{34}$$

3.3 Axial moving harmonic displacement

The time-dependent force at an arbitrary point $d=v_0t$ can be defined as:

$$f_t(x,t)=F_n(t)\delta(x-v_0t)=(f_0\sin\Omega t)\delta(x-v_0t) \tag{35}$$

By substituting Eq. (34) into Eq. (32), the generalized force can be expressed as:

$$\begin{aligned}&F_n(t)=Y_n\int_0^l f_0\sin\Omega t\left(\delta(x-v_0t)-(e_0a)^2\delta''(x-v_0t)\right)U_n(x)dx=\\&Y_nf_0\sin\Omega t\left(U_n(v_0t)-(e_0a)^2U_n''(v_0t)\right)\end{aligned} \tag{36}$$

As it is indicated in Fig. 1, the mode shape for the axial moving load at point *d* can be defined as:

$$U_n(x)=\sqrt{2/l}\sin(Pd)=\sqrt{2/l}\sin(Pv_0t) \tag{37}$$

By replacing Eq. (37) into Eq. (36), the generalized force will be formed as follows:

$$F_n(t)=Y_n\sqrt{2/l}f_0(\sin\Omega t)\sin(Pv_0t)\left(1+(e_0a)^2P^2\right) \tag{38}$$

Replacing Eq. (38) into Eq. (34) in the time domain $0<\tau<t$, causes $q_n(t)$ to be rewritten as:

$$q_n(t)=D_n\int_0^t\sin\Omega\tau\sin(Pv_0\tau)\sin\lambda_n(t-\tau)d\tau \tag{39}$$

Integrating Eq. (39) over time, results in:

$$q_n(t)=D_n\left[\left(2\Psi_n\Omega\left(\cos\lambda_nt-\cos\Omega t\left(\cos\Psi_nt\right)\right)+\left(\lambda_n^2-\Psi_n^2-\Omega^2\right)\left(\sin\Psi_nt\right)\sin\Omega t\right)\right] \tag{40}$$

where

$$D_n=\frac{Y_nf_0\sqrt{2/l}\left(1+(e_0a)^2P^2\right)}{\left(\left(\Psi_n-\Omega\right)^2-\lambda_n^2\right)\left(\left(\Psi_n+\Omega\right)^2-\lambda_n^2\right)} \tag{41}$$

From above, Ψ_n is equivalent to Pv_0 . By multiplication of Eq. (40) by the mode shape in Eq. (28), the axial displacement at point $x=l/2$ can be rewritten as:

$$\begin{aligned}u(x,t)=&\frac{2f_0}{\rho Al}\sum_{n=1}^{\infty}\frac{\sin(Pl/2)}{\left(\left(\Psi_n-\Omega\right)^2-\lambda_n^2\right)\left(\left(\Psi_n+\Omega\right)^2-\lambda_n^2\right)}\\&\times\left(2\Psi_n\Omega\left(\cos\lambda_nt-\cos\Omega t\left(\cos\Psi_nt\right)\right)+\left(\lambda_n^2-\Psi_n^2-\Omega^2\right)\left(\sin\Psi_nt\right)\sin\Omega t\right)\end{aligned} \tag{42}$$

The axial displacement for C-C boundary condition can be defined as:

$$\begin{aligned}u(x,t)=&\frac{2f_0}{\rho Al}\left(\sum_{n=1,3,5,\ldots}^{\infty}\frac{2\Psi_n\Omega\left(\cos\lambda_nt-\cos\Omega t\left(\cos\Psi_nt\right)\right)+\left(\lambda_n^2-\Psi_n^2-\Omega^2\right)\left(\sin\Psi_nt\right)\sin\Omega t}{\left(\left(\Psi_n-\Omega\right)^2-\lambda_n^2\right)\left(\left(\Psi_n+\Omega\right)^2-\lambda_n^2\right)}\right.\\&\left.-\sum_{n=2,4,6,\ldots}^{\infty}\frac{2\Psi_n\Omega\left(\cos\lambda_nt-\cos\Omega t\left(\cos\Psi_nt\right)\right)+\left(\lambda_n^2-\Psi_n^2-\Omega^2\right)\left(\sin\Psi_nt\right)\sin\Omega t}{\left(\left(\Psi_n-\Omega\right)^2-\lambda_n^2\right)\left(\left(\Psi_n+\Omega\right)^2-\lambda_n^2\right)}\right)\end{aligned} \tag{43}$$

Subsequently, the axial displacement for C-F boundary condition can be expressed as:

$$\begin{aligned}u(x,t)=&\frac{2f_0}{\rho Al}\left(\sum_{n=1}^{\infty}\left(\frac{2\Psi_n\Omega\left(\cos\lambda_nt-\cos\Omega t\left(\cos\Psi_nt\right)\right)}{\left(\left(\Psi_n-\Omega\right)^2-\lambda_n^2\right)\left(\left(\Psi_n+\Omega\right)^2-\lambda_n^2\right)}\right.\right.\\&\left.\left.+\frac{\left(\lambda_n^2-\Psi_n^2-\Omega^2\right)\left(\sin\Psi_nt\right)\sin\Omega t}{\left(\left(\Psi_n-\Omega\right)^2-\lambda_n^2\right)\left(\left(\Psi_n+\Omega\right)^2-\lambda_n^2\right)}\right)\times\sin\left(\frac{(2n-1)\pi}{4}\right)\right)\end{aligned} \tag{44}$$

4 NUMERICAL RESULTS

In this part, the numerical results of governed equations from the previous section are discussed. Firstly, the natural frequencies for some various modes and nonlocal parameters are investigated, then in order to prove the accuracy and correctness, the results are compared with those obtained from Mohammadian et al. [61]. In the next part, the dynamic axial vibration under a moving harmonic load is studied at point $x = l/2$. The small-scale effect, also geometrical parameter, and the role of the excitation frequency in the axial displacement is depicted and explained. The amplitude of the harmonic load ($F_t = f_0 \sin \Omega t$) is $f_0 = 1000$; the velocity is considered to be $v_0 = 3\ nm/ns$. In this study, the body is considered as a single-walled carbon nanotube (SWCNT), and the boundary conditions are assumed to be clamped-clamped and clamped-free; the material properties are assumed to be $\rho = 2300\ kg/m^3$, $t = 0.34$, $E = 1\ Tpa$, and $l = 5\ nm$ [79]. With these parameters, the inner, and the outer radii of CNT are $R_{in} = (d - t)/2$ and $R_{out} = (d + t)/2$, respectively. Table. 1 compares the nondimensional axial natural frequencies for three different modes under the C-C and C-F boundary conditions. The results prove that the number of the mode and nonlocal parameter have a direct and inverse effect on the natural frequency, respectively. As the mode number increases, the frequency increases, and as the nonlocal parameter increases the natural frequency decreases. It is due to the fact that the increment in the nonlocal parameter and subsequent reduction of the stiffness causes a decrement in the natural frequency. For the final comprehensible point, it should be announced that the C-C boundary condition, has greater value in comparison with C-F one. It is because of freedom of the action in the opening side for C-F boundary condition.

Table 1

The comparison of the non-dimensional axial vibration $\bar{\omega}_n$ for three various mode shapes and two C-C and C-F boundary condition (l =20 nm).

e_0a (nm)	Mode	Nondimensional axial natural frequencies			
		Present		Ref. [61]	
		CC	CF	CC	CF
0.5	1	3.1319	1.5695	3.1318	1.5697
	3	9.1735	7.7068	9.1732	7.7072
	5	14.6210	13.3292	14.6205	13.3297
1	1	3.1035	1.5659	3.1034	1.5661
	3	8.5255	7.3105	8.5253	7.3108
	5	12.3534	11.5443	12.3532	11.5445

Fig. 3 indicates the effect of the nonlocal parameter on the variation of the axial displacement versus time for two various C-C and C-F boundary conditions. Three various nonlocal parameters are utilized ($\mu = 0\ nm$, $\mu = 1\ nm$, and $2\ nm$). It is obvious that for greater values of the nonlocal parameter, the axial displacement increases due to a decrease in amount of CNT's stiffness. For the identical condition and parameters, the axial displacement is greater for C-F boundary condition. The wavelength is the same for each phase. Based on the local elasticity ($\mu = 0\ nm$), the axial displacement raises over time. When $\mu = 1\ nm$, not only it raises but also variates with a constant slope. The variations of the axial displacement in the time domain for both C-C and C-F boundary conditions and various lengths have been shown in Fig.4. It is observable that for the maximum displacement, the length is in its minimum amount. As CNT's length increases, the axial displacement decreases. For C-F boundary condition, this variation is more sensible. Moreover, the value of the axial displacement is greater for the C-F boundary condition. Another effect of the length is that, the amplitude of the axial displacement variates by the time, when $l = 5\ nm$, for both boundary conditions, but in other states, it just increases. In Fig. 5, the influence of the velocity of the moving load on the variation of the axial displacement versus time is investigated. The nonlocal parameter is equivalent to $\mu = 1\ nm$. The velocity has a direct effect on the axial displacement. The maximum axial displacement increases after each period for greater values of velocity ($v_0 = 20\ nm/ns$). The variation of the axial displacement versus time for three different values of CNT's thicknesses for two types of boundary conditions, including C-C and C-F boundary condition is depicted in Fig. 6. It is distinctly clear that the thickness has an inverse effect on the axial displacement. When thickness is in the lowest amount, the cross-sectional area is greater, and based on Eqs. (42) and (43), the axial displacement will be decreased with a specified discipline for both boundary conditions. It is because of the appearance of the cross-sectional area out of the sigma.

Totally, the axial displacement for the C-F boundary condition is greater than the C-C boundary condition due to the maximum amount of the mode shape at point $x = l/2$ for C-C boundary condition. Fig. 7 illustrates the effect of the ratio of the excitation frequency to natural frequency (Ω / ω_n). The ratio is considered less than one. It is shown that the less the ratio is, the more the axial displacement will be, but when $t < 4\times10^{-4}\ ns$, the axial displacement for greater ratios, has the maximum value. As time passes, the axial displacements will be greater for the lower values of the excitation frequency to natural frequency ratio for both end conditions.

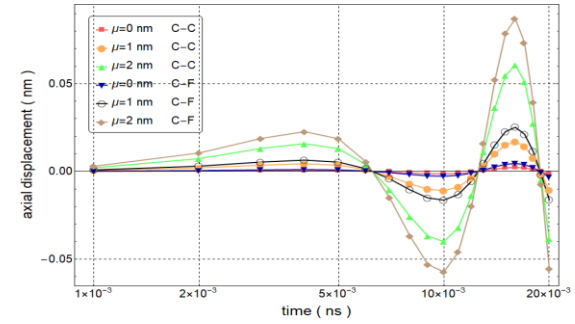

Fig.3
Variation of the axial displacement versus time for various nonlocal parameters ($v_0 = 3\ nm/ns$, and $l = 5$ nm).

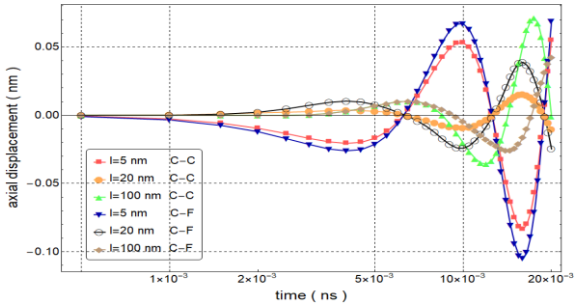

Fig.4
Variation of the axial displacement versus time for various lengths ($v_0 = 3\ nm/ns$, and $\mu = 1\ nm$).

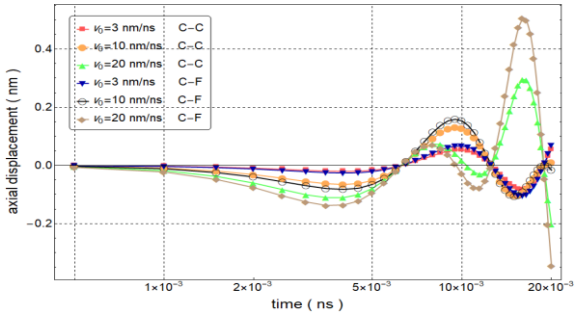

Fig.5
Variation of the axial displacement versus time for various velocities of the moving load ($l = 5$ nm , and $\mu = 1\ nm$).

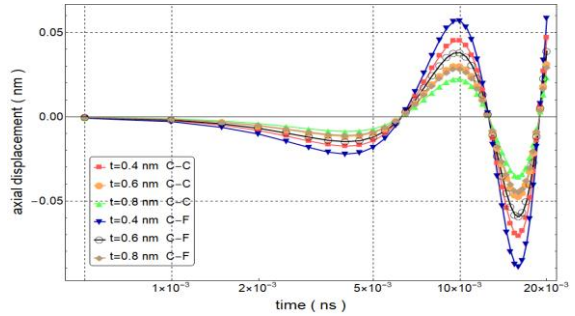

Fig.6
Variation of the axial displacement versus time for various thicknesses ($v_0 = 3\ nm/ns$, $l = 5$ nm and $\mu = 1\ nm$).

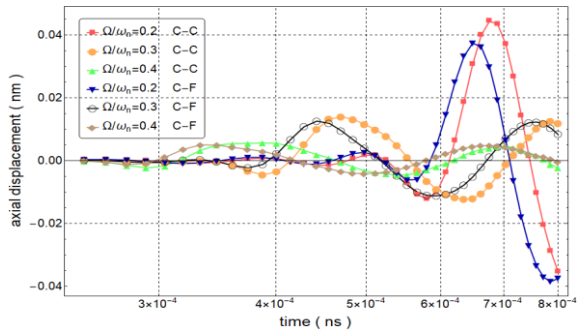

Fig.7
Variation of the axial displacement versus time for various excitation frequency to natural frequency ratios ($v_0 = 3\ nm/ns$, $l = 5$ nm and $\mu = 1\ nm$).

5 CONCLUSION

The dynamic free and forced axial vibrations for a SWCNT due to the axial moving harmonic force was studied based on Eringen's nonlocal elasticity theory in this paper. Two types of boundary conditions, including the clamped-clamped and clamped-free boundary conditions, were considered. By employing Hamilton's principle, the governing equation and corresponding boundary conditions were derived. Via the application of Galerkin's methods, the derived equation was discretized by eliminating the time-dependent force and considering it to calculate the natural frequencies and dynamic axial displacements, respectively. In free axial vibration, it was concluded that the mode number and the nonlocal parameter have a direct and inverse effect on the natural frequency, respectively. The time-dependent axial displacement based on time under a moving harmonic SWCNT was investigated for the first time. The influences of the velocity of the axial moving force and excitation frequency to natural frequency ratio, as well as geometry and small-scale effect on the axial displacement, were illustrated. The nonlocal parameter has a direct effect on the axial displacement, while the thickness has an inverse effect. Also, the axial displacement for C-F boundary condition is greater than C-C one. Increasing the amounts of the length has an inverse effect on the variation of the axial displacement in the time domain. This variation is more sensible for C-F boundary condition. Furthermore, the amounts of the axial displacement are greater for C-F boundary condition. The velocity of the moving load has a direct effect on the axial displacement. Also, the excitation frequency to natural frequency ratio has an inverse effect on the axial displacement.

REFERENCES

[1] Kroto H.W., 1985, C_{60}: Buckminsterfullerene, *Nature* **318**: 162-163.
[2] Krätschmer W., 1990, Solid C_{60}: a new form of carbon, *Nature* **347**: 354-358.
[3] Iijima S., 1991, Synthesis of Carbon Nanotubes, *Nature* **354**: 56-58.
[4] Iijima S., Ichihashi T., 1993, Single-shell carbon nanotubes of 1-nm diameter, *Nature* **363**: 603-605.
[5] Iijima S., 1991, Helical microtubules of graphitic carbon, Nature **354**: 56-58.
[6] Lu X., Chen Z., 2005, Curved pi-conjugation, aromaticity, and the related chemistry of small fullerenes (< C60) and single-walled carbon nanotubes, Chemical Reviews **105**(10): 3643-3696.
[7] Dresselhaus M., 2004, Electronic, thermal and mechanical properties of carbon nanotubes. *Philosophical Transactions of the Royal Society of London, Series A: Mathematical, Physical and Engineering Sciences* **362**: 2065-2098.
[8] Hong S., Myung S., 2007, Nanotube electronics: A flexible approach to mobility, *Nature Nanotechnology* **2**(4): 207-208.
[9] Bethune D., 1993, Cobalt-catalysed growth of carbon nanotubes with single-atomic-layer walls, *Nature* **363**: 605-607.
[10] Dai H., 2002, Carbon nanotubes: opportunities and challenges, *Surface Science* **500** (1-3): 218-241.
[11] De Volder M.F., 2013, Carbon nanotubes: present and future commercial applications, *Science* **339**: 535-539.
[12] Esawi A.M., Farag M.M., 2007, Carbon nanotube reinforced composites: potential and current challenges, *Materials & Design* **28**(9): 2394-2401.
[13] Mubarak N., 2014, An overview on methods for the production of carbon nanotubes, *Journal of Industrial and Engineering Chemistry* **20**(4): 1186-1197.
[14] Lei Z., Zhang L., Liew K., 2015, Free vibration analysis of laminated FG-CNT reinforced composite rectangular plates using the kp-Ritz method, *Composite Structures* **127**: 245-259.
[15] Zhang L., Song Z., Liew K., 2015, State-space Levy method for vibration analysis of FG-CNT composite plates subjected to in-plane loads based on higher-order shear deformation theory, *Composite Structures* **134**: 989-1003.

[16] Natarajan S., Haboussi M., Manickam G., 2014, Application of higher-order structural theory to bending and free vibration analysis of sandwich plates with CNT reinforced composite facesheets, *Composite Structures* **113**: 197-207.
[17] Wang Z.-X., Shen H.-S., 2012, Nonlinear vibration and bending of sandwich plates with nanotube-reinforced composite face sheets, *Composites Part B: Engineering* **43**(2): 411-421.
[18] Ma J., 2010, Diameters of single-walled carbon nanotubes (SWCNTs) and related nanochemistry and nanobiology, *Frontiers of Materials Science in China* **4**(1): 17-28.
[19] Sethuraman A., Stroscio M.A., Dutta M., 2004, *Potential Applications of Carbon Nanotubes in Bioengineering*, Springer.
[20] Chen Y., Zhang J., 2014, Chemical vapor deposition growth of single-walled carbon nanotubes with controlled structures for nanodevice applications, *Accounts of Chemical Research* **47**(8): 2273-2281.
[21] Fukuda T., Arai F., Dong L., 2003, Assembly of nanodevices with carbon nanotubes through nanorobotic manipulations, *Proceedings of the IEEE* **91**(11): 1803-1818.
[22] Ma P.-C., 2010, Dispersion and functionalization of carbon nanotubes for polymer-based nanocomposites: a review, *Composites Part A: Applied Science and Manufacturing* **41**(10): 1345-1367.
[23] Sahoo N.G., 2010, Polymer nanocomposites based on functionalized carbon nanotubes, *Progress in Polymer Science* **35**(7): 837-867.
[24] Zarepour M., Hosseini S.A., Ghadiri M., 2017, Free vibration investigation of nano mass sensor using differential transformation method, *Applied Physics A* **123**(3): 181.
[25] Namvar M., 2017, Experimental and analytical investigations of vibrational behavior of U-shaped atomic force microscope probe considering thermal loading and the modified couple stress theory, *The European Physical Journal Plus* **132**(6): 247.
[26] Sourki R., Hosseini S.A., 2017, Coupling effects of nonlocal and modified couple stress theories incorporating surface energy on analytical transverse vibration of a weakened nanobeam, *The European Physical Journal Plus* **132**(4): 184.
[27] Refaeinejad V., Rahmani O., Hosseini S.A., 2017, Evaluation of nonlocal higher order shear deformation models for the vibrational analysis of functionally graded nanostructures, *Mechanics of Advanced Materials and Structures* **24**(13): 1116-1123.
[28] Rahmani O., Hosseini S.A., Parhizkari M., 2017, Buckling of double functionally-graded nanobeam system under axial load based on nonlocal theory: an analytical approach, *Microsystem Technologies* **23**(7): 2739-2751.
[29] Hayati H., Hosseini S.A., Rahmani O.,2016, Coupled twist–bending static and dynamic behavior of a curved single-walled carbon nanotube based on nonlocal theory, *Microsystem Technologies* **23**: 2393-2401.
[30] Eringen A.C., Edelen D., 1972, On nonlocal elasticity, *International Journal of Engineering Science* **10**(3): 233-248.
[31] Eringen A.C., 1983, On differential equations of nonlocal elasticity and solutions of screw dislocation and surface waves, *Journal of Applied Physics* **54**(9): 4703-4710.
[32] Kahrobaiyan M., 2010, Investigation of the size-dependent dynamic characteristics of atomic force microscope microcantilevers based on the modified couple stress theory, *International Journal of Engineering Science* **48**(12): 1985-1994.
[33] Ansari R., 2015, Surface stress effect on the vibration and instability of nanoscale pipes conveying fluid based on a size-dependent Timoshenko beam model, *Acta Mechanica Sinica* **31**(5): 708-719.
[34] Farajpour M.R., 2016, Vibration of piezoelectric nanofilm-based electromechanical sensors via higher-order non-local strain gradient theory, *Micro & Nano Letters* **11**(6): 302-307.
[35] Behrouz S.J., Rahmani O., Hosseini S.A., 2019, On nonlinear forced vibration of nano cantilever-based biosensor via couple stress theory, *Mechanical Systems and Signal Processing* **128**: 19-36.
[36] Hosseini S.A., Rahmani O., 2018, Modeling the size effect on the mechanical behavior of functionally graded curved micro/nanobeam, *Thermal Science and Engineering* **1**(2): 1-20.
[37] Rahmani O., 2018, Size dependent bending analysis of micro/nano sandwich structures based on a nonlocal high order theory, *Steel and Composite Structures* **27**(3): 371-388.
[38] Rahmani O., 2018, Free vibration of deep curved FG nano-beam based on modified couple stress theory, *Steel and Composite Structures* **26**(5): 607-620.
[39] Rahmani O., 2018, Dynamic response of a single-walled carbon nanotube under a moving harmonic load by considering modified nonlocal elasticity theory, *The European Physical Journal Plus* **133**(2): 42.
[40] Ghadiri M., 2018, In-Plane and out of plane free vibration of U-shaped AFM probes based on the nonlocal elasticity, *Journal of Solid Mechanics* **10**(2): 285-299.
[41] Hosseini S.A., Rahmani O., 2018, Bending and vibration analysis of curved FG nanobeams via nonlocal Timoshenko model, *Smart Construction Research* **2**(2): 1-17.
[42] Xu K., Guo X., Ru C., 2006, Vibration of a double-walled carbon nanotube aroused by nonlinear intertube van der Waals forces, *Journal of Applied Physics* **99**(6): 064303.
[43] Lee H.-L., Chang W.-J., 2009, Vibration analysis of a viscous-fluid-conveying single-walled carbon nanotube embedded in an elastic medium, *Physica E: Low-Dimensional Systems and Nanostructures* **41**(4): 529-532.
[44] Moradi-Dastjerdi R., 2014, Vibration analysis of functionally graded nanocomposite cylinders reinforced by wavy carbon nanotube based on mesh-free method, *Journal of Composite Materials* **48**(15): 1901-1913.
[45] Pourseifi M., Rahmani O., Hoseini S.A., 2015, Active vibration control of nanotube structures under a moving nanoparticle based on the nonlocal continuum theories, *Meccanica* **50**(5): 1351-1369.

[46] Mahdavi M., Jiang L., Sun X., 2011, Nonlinear vibration of a double-walled carbon nanotube embedded in a polymer matrix, *Physica E: Low-Dimensional Systems and Nanostructures* **43**(10): 1813-1819.
[47] Kiani K., 2010, Free longitudinal vibration of tapered nanowires in the context of nonlocal continuum theory via a perturbation technique, *Physica E: Low-Dimensional Systems and Nanostructures* **43**(1): 387-397.
[48] Askari H., Esmailzadeh E., Zhang D., 2014, Nonlinear vibration analysis of nonlocal nanowires, *Composites Part B: Engineering* **67**: 607-613.
[49] Ansari R., Torabi J., Shojaei M.F., 2017, Buckling and vibration analysis of embedded functionally graded carbon nanotube-reinforced composite annular sector plates under thermal loading, *Composites Part B: Engineering* **109**: 197-213.
[50] Yas M., Heshmati M., 2012, Dynamic analysis of functionally graded nanocomposite beams reinforced by randomly oriented carbon nanotube under the action of moving load, *Applied Mathematical Modelling* **36**(4): 1371-1394.
[51] Şimşek M., 2010, Vibration analysis of a single-walled carbon nanotube under action of a moving harmonic load based on nonlocal elasticity theory, *Physica E: Low-Dimensional Systems and Nanostructures* **43**(1): 182-191.
[52] Malekzadeh P., Zarei A., 2014, Free vibration of quadrilateral laminated plates with carbon nanotube reinforced composite layers, *Thin-Walled Structures* **82**: 221-232.
[53] Joshi A.Y., Harsha S., Sharma S.C., 2010, Vibration signature analysis of single walled carbon nanotube based nanomechanical sensors, *Physica E: Low-Dimensional Systems and Nanostructures* **42**(8): 2115-2123.
[54] Aydogdu M., 2012, Axial vibration analysis of nanorods (carbon nanotubes) embedded in an elastic medium using nonlocal elasticity, *Mechanics Research Communications* **43**: 34-40.
[55] Aydogdu M., 2015, A nonlocal rod model for axial vibration of double-walled carbon nanotubes including axial van der Waals force effects, *Journal of Vibration and Control* **21**(16): 3132-3154.
[56] Murmu T., Adhikari S., 2010, Nonlocal effects in the longitudinal vibration of double-nanorod systems, *Physica E: Low-Dimensional Systems and Nanostructures* **43**(1): 415-422.
[57] Şimşek M., 2012, Nonlocal effects in the free longitudinal vibration of axially functionally graded tapered nanorods, *Computational Materials Science* **61**: 257-265.
[58] Murmu T., Adhikari S., 2011, Axial instability of double-nanobeam-systems, *Physics Letters A* **375**(3): 601-608.
[59] Danesh M., Farajpour A., Mohammadi M., 2012, Axial vibration analysis of a tapered nanorod based on nonlocal elasticity theory and differential quadrature method, *Mechanics Research Communications* **39**(1): 23-27.
[60] Filiz S., Aydogdu M., 2010, Axial vibration of carbon nanotube heterojunctions using nonlocal elasticity, *Computational Materials Science* **49**(3): 619-627.
[61] Mohammadian M., Abolbashari M.H., Hosseini S.M., 2019, Axial vibration of hetero-junction CNTs mass nanosensors by considering the effects of small scale and connecting region: An analytical solution, *Physica B: Condensed Matter* **553**: 137-150.
[62] Liu K.-C., Friend J., Yeo L., 2009, The axial–torsional vibration of pretwisted beams, *Journal of Sound and Vibration* **321**(1-2): 115-136.
[63] Aydogdu M., Filiz S., 2011, Modeling carbon nanotube-based mass sensors using axial vibration and nonlocal elasticity, *Physica E: Low-Dimensional Systems and Nanostructures* **43**(6): 1229-1234.
[64] Bouadi A., 2018, A new nonlocal HSDT for analysis of stability of single layer graphene sheet, *Advances in Nano Research* **6**(2): 147-162.
[65] Hamza-Cherif R., 2018, Vibration analysis of nano beam using differential transform method including thermal effect, *Journal of Nano Research* **54**: 1-14.
[66] Kadari B., 2018, Buckling analysis of orthotropic nanoscale plates resting on elastic foundations, *Journal of Nano Research* **55**: 42-56.
[67] Yazid M., 2018, A novel nonlocal refined plate theory for stability response of orthotropic single-layer graphene sheet resting on elastic medium, *Smart Structures and Systems* **21**(1): 15-25.
[68] Youcef D.O., 2018, Dynamic analysis of nanoscale beams including surface stress effects, *Smart Structures and Systems* **21**(1): 65-74.
[69] Draoui A., 2019, Static and dynamic behavior of nanotubes-reinforced sandwich plates using (FSDT), *Journal of Nano Research* **57**: 117-135.
[70] Mokhtar Y., 2018, A novel shear deformation theory for buckling analysis of single layer graphene sheet based on nonlocal elasticity theory, *Smart Structures and Systems* **21**(4): 397-405.
[71] Boutaleb S., 2019, Dynamic analysis of nanosize FG rectangular plates based on simple nonlocal quasi 3D HSDT, *Advances in Nano Research* **7**(3): 189-206.
[72] Karami B., 2018, A size-dependent quasi-3D model for wave dispersion analysis of FG nanoplates, *Steel and Composite Structures* **28**(1): 99-110.
[73] Karami B., Janghorban M., Tounsi A.,2018, Nonlocal strain gradient 3D elasticity theory for anisotropic spherical nanoparticles, *Steel and Composite Structures* **27**(2): 201-216.
[74] Karami B., Janghorban M., Tounsi A., 2018, Variational approach for wave dispersion in anisotropic doubly-curved nanoshells based on a new nonlocal strain gradient higher order shell theory, *Thin-Walled Structures* **129**: 251-264.
[75] Bellifa H., 2017, A nonlocal zeroth-order shear deformation theory for nonlinear postbuckling of nanobeams, *Structural Engineering and Mechanic*s **62**(6): 695-702.

[76] Karami B., Janghorban M., Tounsi A., 2017, Effects of triaxial magnetic field on the anisotropic nanoplates, *Steel and Composite Structures* **25**(3): 361-374.
[77] Bouafia K., 2017, A nonlocal quasi-3D theory for bending and free flexural vibration behaviors of functionally graded nanobeams, *Smart Structures and Systems* **19**(2): 115-126.
[78] Zemri A., 2015, A mechanical response of functionally graded nanoscale beam: an assessment of a refined nonlocal shear deformation theory beam theory, *Structural Engineering and Mechanics* **54**(4): 693-710.
[79] Şimşek M., 2011, Nonlocal effects in the forced vibration of an elastically connected double-carbon nanotube system under a moving nanoparticle, *Computational Materials Science* **50**(7): 2112-2123.